# Energy loss of proton, $\alpha$ particle, and electron beams in hafnium dioxide films

Moni Behar,[1] Raul C. Fadanelli,[1] Isabel Abril,[2] Rafael Garcia-Molina,[3] Cristian D. Denton,[2] Luiz C. C. M. Nagamine,[1] and Néstor R. Arista[4]

[1]*Instituto de Fisica, Universidade Federal do Rio Grande do Sul, Av. Bento Gonçalves 9500, 91501-970 Porto Alegre, RS, Brazil*

[2]*Departament de Física Aplicada, Universitat d´Alacant, Apartat 99, E-03080 Alacant, Spain*

[3]*Departamento de Física-CIOyN, Universidad de Murcia, Apartado 4021, E-30080 Murcia, Spain*

[4]*División Colisiones Atómicas, Centro Atómico Bariloche, RA-8400 San Carlos de Bariloche, Argentina*

(Received 24 July 2009; published 4 December 2009)

The electronic stopping power, $S$, of $HfO_2$ films for proton and alpha particle beams has been measured and calculated. The experimental data have been obtained by the Rutherford backscattering technique and cover the range of 120–900 and 120–3000 keV for proton and alpha particle beams, respectively. Theoretical calculations of the energy loss for the same projectiles have been done by means of the dielectric formalism using the Mermin energy loss function—generalized oscillator strength (MELF-GOS) model for a proper description of the $HfO_2$ target on the whole momentum-energy excitation spectrum. At low projectile energies, a nonlinear theory based on the extended Friedel sum rule has been employed. The calculations and experimental measurements show good agreement for protons and a quite good one for alpha particles. In particular, the experimental maximums of both stopping curves (around 120 and 800 keV, respectively) are well reproduced. On the basis of this good agreement, we have also calculated the inelastic mean-free path (IMFP) and the stopping power for electrons in $HfO_2$ films. Our results predict a minimum value of the IMFP and a maximum value of the $S$ for electrons with energies around 120 and 190 eV, respectively.

DOI: 10.1103/PhysRevA.80.062901 PACS number(s): 34.50.Bw

## I. INTRODUCTION

The interaction between energetic charged particles and matter has been investigated extensively both experimentally and theoretically since it concerns a topic of considerable fundamental and applied interests. The energy loss of swift ions is one of the most relevant aspects of this interaction and plays a central role in various areas such as microelectronics, materials science, nuclear and plasma physics, radiation detectors, cancer therapy, and space exploration [1].

Measurements of stopping power represent a demanding work due to the variety of incident projectiles and energies (covering several orders of magnitude) and the complexity of the irradiated targets. Significant effort is required to know the stopping power in the region around its maximum value and in the low-energy range for a given medium because the characteristics of projectile-target electron interactions change, which makes it difficult for a theoretical treatment. In addition, available experimental data in this energy range are scarce or inexistent for interesting projectile-target combinations.

Continued miniaturization of sizes in complementary metal-oxide-semiconductor (CMOS) integrated circuits requires the replacement of $SiO_2$ as gate dielectric by alternative high-dielectric-constant materials [2–4]. Hafnium dioxide ($HfO_2$) is one of the most promising candidates, which already started to replace silicon dioxide in microelectronic technology due to its high dielectric constant. In addition, $HfO_2$ has been used in optical coating applications and is a potential candidate for energy-saving devices [5,6]. Other uses of $HfO_2$ are found in gas and magnetic sensors. Therefore, due to the high technological interest on $HfO_2$ films, a large research effort is necessary in order to connect the physical properties of this material with the manufacturing conditions, aiming to find the optimal deposition process and parameters for a given application.

In order to measure the thickness of $HfO_2$ films and to predict or simulate range profiles for implantation [7], the experimental determination of the stopping power of ion beams in $HfO_2$ is of significant interest. So, knowledge of how swift projectiles (ions or electrons) lose energy in $HfO_2$ films is highly necessary.

However, the availability of ion stopping data in compounds is very limited due to experimental difficulties in preparing and handling compound targets for energy-loss measurements. To the best of our knowledge, the stopping power of light ions, such as H and He beams, into $HfO_2$ has never been measured and only recently the energy-loss straggling has been experimentally obtained [8].

Additionally, due to the potential use of $HfO_2$ films as a gate dielectric, the transport of electrons through such material must be well characterized. This requires knowledge of two main quantities: the stopping power and the inelastic mean-free path (IMFP) of electrons in a wide range of energies.

In this work, we present the experimental results of the stopping power for H and He ion beams in $HfO_2$ films obtained using the Rutherford backscattering technique. In addition, we have also evaluated these magnitudes using two different approaches: (i) calculations based in the dielectric formalism, paying especial attention to a proper description of the electronic properties of the $HfO_2$ films [9,10], valid at medium and high projectile energies, and (ii) a nonlinear model based in the extended Friedel sum rule, which is appropriate at low projectile velocities [11]. We have compared the experimental results to the theoretical ones and the agreement resulted to be quite good.

Finally, we show calculations of the inelastic mean-free path and stopping power of $HfO_2$ for electrons in a wide

 ©2009 The American Physical Society

incident-energy range. Besides their intrinsic value, these results serve to validate theoretical predictions [12,13] for the energy loss and the mean-free paths of electrons in $HfO_2$, but unfortunately up to now, there are no experimental results to be compared to.

## II. EXPERIMENTAL PROCEDURE

### A. Sample preparation

The $HfO_2$ films were grown on a Si (100) substrate by radio frequency magnetron sputtering (150 W) using a $HfO_2$ target with a nominal purity of 99.95% and $O_2$/Ar flow ratio gas mixture as sputtering gas. The sputtering system was evacuated to $8.0\times10^{-8}$ Torr by a turbo molecular pump backed by a mechanical pump before the deposition. The total work pressure was 5.7 mTorr during the deposition, with an Ar gas flow of 19.6 sccm (sccm denotes cubic centimeter per minute at STP) and an $O_2$/Ar ratio flow of 0.35. The deposition rate (3.3 nm/min) was checked by the analysis of low-angle x-ray reflectivity scan on one of the $HfO_2$ films and the thicknesses ($t$=17, 32, 63, 72, and 91 nm) of the $HfO_2$ films were controlled using the deposition time and after check by the x-ray reflectivity technique. A Phillips X-Pert $\theta$-$2\theta$ diffractometer employing Cu $K\alpha$ radiation was used to obtain the low- and high-angle diffraction scans. The typical error in the thickness determination was of the order of 5%. The stoichiometry of the films was checked and confirmed by using the Rutherford backscattering (RBS) technique.

### B. RBS measurements

The energy losses of H and He in $HfO_2$ were determined by means of the Rutherford backscattering technique using the ion beams provided by the 500 kV ion implanter (for the lower energies) and the 3 MV Tandetron (for the higher ones). These experiments were carried out at the Instituto de Fisica da Universidade Federal do Rio Grande do Sul (IF-UFRGS), Brazil.

For the H beam, the interval of energy covered by the present experiment was between 120 and 900 keV and the total detector plus electronic resolution was of the order of 7 keV (full width at half maximum, FWHM). For the He case, the investigated energies range from 120 to 3000 keV and the combined electronic plus detector resolution was 12 keV (FWHM).

The sample was mounted on a four-axis goniometer. The detector position was fixed at 120° with respect to the beam direction, being 2 millisteradian its aperture. For each incident energy, the angle between the beam and the normal to the sample was varied between 0° and 60°. A typical RBS spectrum resulting from the 72 nm $HfO_2$ target taken with a He ion beam at 1 MeV is shown in Fig. 1. The selection of the sample thicknesses was done according to the energy of the beam. Moreover, in several occasions we have performed the experiment at a fixed energy changing the samples and the obtained results were quite similar, independent of the thickness of the film under analysis. It should be stressed that the energy stabilities of the Tandetron accelerator as well as

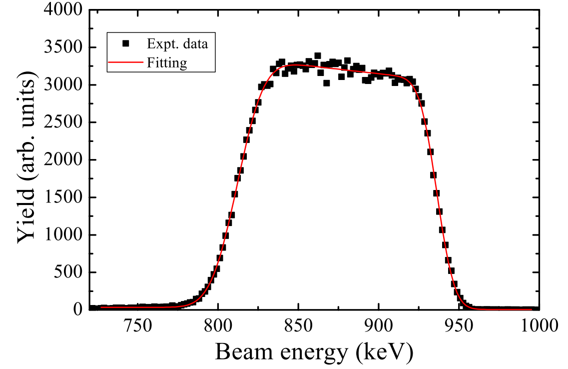


FIG. 1. (Color online) A typical RBS spectrum resulting from a 72-nm-thick $HfO_2$ target taken with a He ion beam at 1 MeV. The symbols correspond to experimental data, while the line is a fitting to these data.

the ion implanter are very good (better than 0.1%) and the typical RBS currents were of the order of 10–15 nA in order to avoid pile-up problems

### C. Data analysis

The energy loss $\Delta E$ of the H and He ions in a $\Delta x$-thick $HfO_2$ layer was evaluated by determining the position of the edges of the corresponding energy distribution. Since the maximum energy transferred in a single process is much smaller than the energy-loss straggling, following Bohr criterion [14], the energy-loss distribution has a Gaussian shape. As the experimental resolution is also Gaussian-like, the back edge of the energy distribution can be fitted with the error function and the leading edge with the complementary error function.

The stopping power $dE/dx$ can be obtained from the experimental data for the ions backscattered at a depth $x$ of the film, through the following relation based on the mean-energy approximation [15]:

$$\Delta E(x) = \frac{xK}{\cos\theta_1}\left.\frac{dE}{dx}\right|_{\bar{E}_{in}} + \frac{x}{\cos\theta_2}\left.\frac{dE}{dx}\right|_{\bar{E}_{out}}, \qquad (1)$$

where $K$ is the kinematic factor, $\theta_1$ and $\theta_2$ are the angles of the sample normal to the incoming beam and the detector position, respectively, and $dE/dx|_{\bar{E}_{in}(\bar{E}_{out})}$ is the stopping power of $HfO_2$ for the H or He ions of energy $\bar{E}_{in}(\bar{E}_{out})$.

In the mean-energy approximation, it is assumed that the energies along the inward ($\bar{E}_{in}$) and outward ($\bar{E}_{out}$) paths are $\bar{E}_{in}=(E+E_0)/2$ and $\bar{E}_{out}=(K\cdot E+E_1)/2$, respectively, where $E_0$ is the energy of the incident particles, $E$ is the energy immediately before scattering at a depth $x$, and $E_1$ is the energy of the backscattered particles emerging from the surface. For each spectrum, $E$ was determined using the energy-loss ratio method as described in Ref. [15].

Considering Eq. (1) for ions backscattered at the back of the $HfO_2$ film, with $x$ equal to the film thickness $\Delta x$, when measuring at two (or more) different geometries, a system of equations is obtained, which can be solved to get the stopping power values $dE/dx|_{\bar{E}_{in}}$ and $dE/dx|_{\bar{E}_{out}}$. For each energy

$E_0$, four measurements were performed under different geometrical conditions ($\theta_1=0°$, 20°, 40°, and 60°; $\theta_2=60°-\theta_1$). The stopping power and their corresponding energies $\bar{E}_{in}$ and $\bar{E}_{out}$ were taken as the mean values of the results. Proceeding in the same way for each energy, the stopping power data for H and He were obtained [16]. The main source of errors is due to the dispersion between the different values obtained for a fixed energy at different angles and film thicknesses.

## III. THEORETICAL CALCULATIONS FOR H AND HE PROJECTILES

Two approaches, a linear theory and a nonlinear one, have been used to study the electronic energy loss of light ions in $HfO_2$ films. The former is the dielectric formalism [17], which is based on first-order perturbation theory. However, at low projectile velocities, it is necessary to incorporate higher-order effects [18], therefore a nonlinear theory based in the extended Friedel sum rule [11] has been employed in this case.

### A. Dielectric approach

The dielectric formalism is useful to describe the electronic interaction of fast-charged particles in solids since it includes in a self-consistent way the screening of the incident projectile together with the individual and collective target electron excitations [17]. The stopping power, $S_q$, of an ion with charge $q$, atomic number $Z_1$, and velocity $v$, moving through a solid with a dielectric constant, $\varepsilon(k,\omega)$, can be written as [10]

$$S_q = \frac{2e^2}{\pi v^2}\int_0^\infty d\omega\omega\int_{\omega/v}^\infty \frac{dk}{k}|f_q(k)|^2 \mathrm{Im}\left[\frac{-1}{\varepsilon(k,\omega)}\right], \quad (2)$$

where $\hbar k$ and $\hbar\omega$ represent the momentum and energy transferred to the target electrons in an elementary inelastic process. $f_q(k)$ is the Fourier transform of the projectile charge density for the charge state $q$; here, we use the statistical model developed by Brandt and Kitagawa [19].

Due to the electron capture and loss by the projectile, the total stopping power $S$ will be a linear combination of the stopping power associated to each charge state $q$ of the projectile, that is,

$$S = \sum_{q=0}^{Z_1} \phi_q S_q. \quad (3)$$

Here, $\phi_q$ represents the equilibrium $q$-charge state fractions of the projectile at each velocity $v$. We take $\phi_q$ values from a parameterization provided by the CASP code [20], although for compound targets, this code applies Bragg's rule [21] to the target constituents.

To calculate the stopping power from Eq. (2), we need a suitable description of the energy-loss function (ELF) of the target, $\mathrm{Im}[-1/\varepsilon(k,\omega)]$. We applied the Mermin energy loss function—generalized oscillator strength (MELF-GOS) method [9,10] to describe the ELF of $HfO_2$ since it has been successfully used to describe the ELF of materials with a complex electronic spectrum [22–24]. Contributions of the outer- and inner-shell electrons to the excitation spectrum are treated separately according to the following expression:

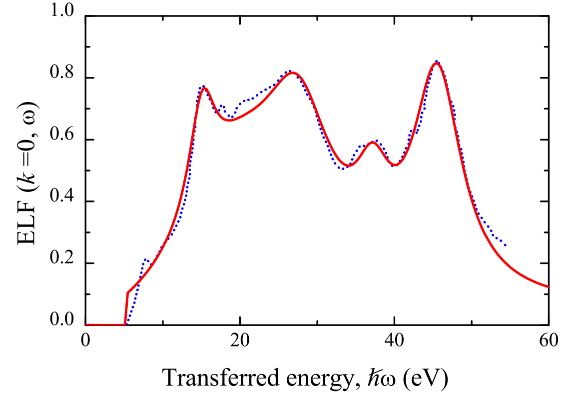


FIG. 2. (Color online) Energy loss function of $HfO_2$ as a function of the transferred energy, $\hbar\omega$, in the optical limit ($k$=0). The dotted line corresponds to experimental data from Frandon *et al.* [27], while the solid line represents the ELF obtained through the MELF-GOS model.

$$\mathrm{Im}\left[\frac{-1}{\varepsilon(k=0,\omega)}\right] = \sum_i A_i \,\mathrm{Im}\left[\frac{-1}{\varepsilon_M(\omega_i,\gamma_i;k=0,\omega)}\right] \times\Theta(\omega-\omega_{th,i}) + \frac{2\pi N}{\omega}\sum_j \alpha_j \sum_{nl}\frac{df_{nl}^{(j)}(k,\omega)}{d\omega}. \quad (4)$$

The first term corresponds to the outer-electron excitations, which are fitted to the experimental optical spectrum ($k$=0) through a linear combination of Mermin-type ELF [25]; $\omega_i$, $\gamma_i$, and $A_i$ are, respectively, the plasma frequency, width, and intensity of the most relevant peaks in the experimental spectrum and $\omega_{th,i}$ is a threshold energy.

The second term in Eq. (4) takes into account the inner-shell electron excitations, described by their GOSs, where $N$ is the molecular density of the target, $df_{nl}^{(j)}(k,\omega)/d\omega$ is the GOS of the $(n,l)$ subshell of the $j$th element, and $\alpha_j$ indicates the $j$th element stoichiometry in the target. For $HfO_2$ films, the electrons from the $K$ shell of O as well as the $K$, $L$ and $M$ shells of Hf are treated as inner electrons. We assume a nonrelativistic GOS in the hydrogenic approach. We have also checked that a more sophisticated GOS (relativistic and nonhydrogenic approach) has a negligible influence in the stopping power [26].

In Fig. 2, we show the experimental energy-loss function of $HfO_2$ at $k$=0 as a function of the transferred energy, obtained by Frandon *et al.* [27]. This spectrum reflects the richness and complexity of transition metals and it has been interpreted in terms of interband transitions at low energy, transitions to high-lying empty states, excitations of core levels, and collective excitations [28,29]. The ELF obtained from the MELF-GOS model, Eq. (4), is also shown with the parameters given in Table I. We demand to the MELF-GOS method the fulfillment of the $f$-sum rule at any transferred

TABLE I. Parameters used in Eq. (4) to describe the contribution of the outer electrons to the ELF spectrum of $HfO_2$. $\hbar\omega_{th,i}$ =5.5 eV corresponds to the gap energy [46].

| $i$ | $\hbar\omega_i$ (eV) | $\hbar\gamma_i$ (eV) | $A_i$ |
|---|---|---|---|
| 1 | 15.2 | 4.2 | $9.57\times 10^{-2}$ |
| 2 | 21.2 | 16.3 | $2.96\times 10^{-1}$ |
| 3 | 28.0 | 10.9 | $1.98\times 10^{-1}$ |
| 4 | 37.3 | 5.4 | $3.46\times 10^{-2}$ |
| 5 | 45.7 | 7.6 | $1.17\times 10^{-1}$ |
| 6 | 102 | 218 | $7.82\times 10^{-2}$ |
| 7 | 403 | 721 | $6.39\times 10^{-3}$ |

momentum; namely, the effective number of target electrons, $N_{\text{eff}}$, that participate in excitations or ionizations up to a transferred energy $\hbar\omega$,

$$N_{\text{eff}}(\hbar\omega) = \frac{m}{2\pi^2 e^2 N}\int_0^{\omega} d\omega'\,\omega'\;\text{Im}\left[\frac{-1}{\varepsilon(k=0,\omega')}\right], \quad (5)$$

must tend to the total number of target electrons when $\hbar\omega \to \infty$. In the above expression, $m$ is the electron mass. For $HfO_2$ films, the $f$-sum rule is achieved better than 0.1%. One of the advantages of the Mermin-type ELF is that the $f$-sum rule, checked at $k=0$, is automatically satisfied for all values of the momentum transfer $k$. However, due to Pauli's exclusion principle, the effective number of electrons of the inner shells (described by the GOS) depends on the momentum transfer $k$ because there is a transfer of GOS from the deeper shells to the external ones, and only at $\hbar k \to \infty$ these electrons behave as free and therefore $N_{\text{eff}}$ will be equal to the number of electrons of each shell. Due to this fact, the first term in Eq. (4) must be modulated by a factor that depends on $k$ to guarantee that the $f$-sum rule must be verified at any transferred momentum. In Fig. 3, we show the effective number of electrons as a function of the transferred energy

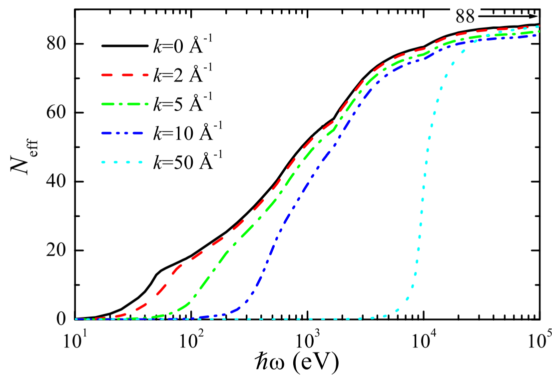


FIG. 3. (Color online) Effective number of electrons, $N_{\text{eff}}$, of $HfO_2$ as a function of the maximum transferred energy for several values of $k$: 0 Å$^{-1}$ (solid line), 2 Å$^{-1}$ (dashed line), 5 Å$^{-1}$ (dash-dotted line), 10 Å$^{-1}$ (dash-dot-dotted line), and 50 Å$^{-1}$ (dotted line). The arrow points to 88, which is the total number of electrons of $HfO_2$.

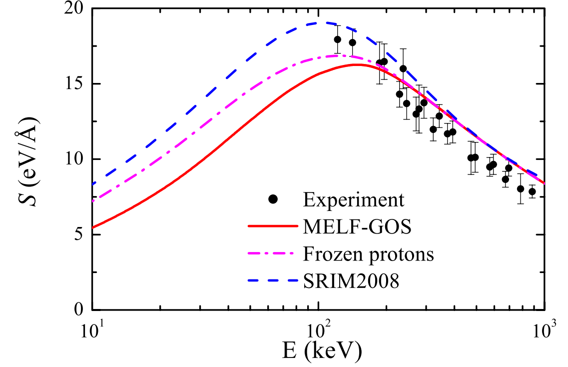


FIG. 4. (Color online) Stopping power of $HfO_2$ for a H beam as a function of the incident projectile energy. Experimental data obtained in this work are shown by symbols; results from the dielectric MELF-GOS model are represented by a solid line, while the dash-dotted line corresponds to frozen protons. The results provided by the SRIM 2008 code [32] are depicted by a dashed line.

for several values of $k$ (0, 2, 5, 10, and 50 Å$^{-1}$). As we can see, when $\hbar\omega \to \infty$, the effective number of electrons tends to the total number of target electrons, independently of the momentum transfer, which is 88. The mean excitation energy, $I$, obtained from the MELF-GOS method gives a value of $I(HfO_2)=414$ eV for $HfO_2$ films, which is ~20% smaller than the value $I(HfO_2)=552$ eV derived by interpolation from the ICRU report [30].

### B. Nonlinear method

This method includes three basic aspects (cf. [11,31]). First, the screening of the ion by the target valence electrons is represented, in terms of the appropriate phase shifts, using quantum-scattering theory and performing numerical integrations of the Schrödinger equation to calculate the phase-shift values. Secondly, the scattering potential is adjusted in a self-consistent way, for each ion velocity, using the extended Friedel sum rule (EFSR), which yields a condition on the phase shifts. Then, the momentum-transfer cross section is calculated, as a function of the relative electron-ion velocity (and for each ion velocity of interest), using the phase-shift values. Finally, a complete integration over relative velocities is performed (considering for each integration a given ion velocity, $v$, and a Fermi-sphere distribution for the valence electron velocities). This procedure is repeated for each ion charge state and produces a partial-stopping curve for each case (for the He projectile, the stopping powers for $He^0$, $He^+$, and $He^{2+}$ are obtained). Later on, the total nonlinear stopping power will be obtained by an average over the projectile charge state fractions [see Eq. (3)].

## IV. RESULTS AND DISCUSSION FOR ION PROJECTILES

The experimental stopping power of $HfO_2$ for H beams is depicted in Fig. 4 as a function of the projectile energy, which ranges from 120 to 900 keV. The experimental points seem to indicate that the stopping power maximum occurs in the region around 100–120 keV. The solid curve is the result obtained with the dielectric formalism together with the

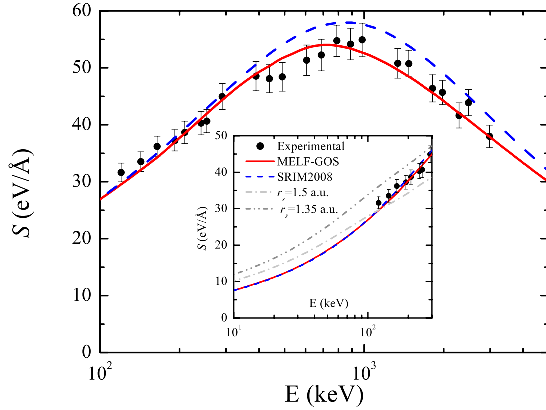


FIG. 5. (Color online) Stopping power of $HfO_2$ for a He beam as a function of the incident projectile energy. Experimental data are shown by black symbols; results from the dielectric MELF-GOS model are depicted by a solid line, while the dashed line represents values from SRIM2008 code [32]. In the inset, we also plot, by means of gray lines, the results corresponding to the nonlinear model for several values of the $r_s$ parameter.

MELF-GOS model to describe the $HfO_2$ target response. We observe that the maximum of the stopping power occurs at around 120 keV as suggested by the experimental results. The dash-dotted curve represents the same calculation but assuming that the H projectiles behave as protons with a frozen charge state. At large projectile energies, both curves coincide because the charge state for all H projectiles corresponds to protons. However, around and below the stopping power maximum, the fraction of neutrals increases, which produces a smaller stopping power as compared to that of a frozen proton. In this sense, the stopping power of a frozen proton represents an upper limit to the stopping power, inasmuch as the charge fractions of a compound are not fully known. It is interesting to emphasize that most of the contribution to the stopping power comes from the outer-shell electrons described by Mermin-type ELF, whereas the contribution from the oxygen $K$ shell or the hafnium $K$, $L$, and $M$ shells is negligible in this energy range.

The agreement between theory and experiments is quite good considering the experimental-error limits. Around the stopping power maximum, some differences arise which could be attributed to possible errors in the charge fractions used or to nonlinear terms not included in the dielectric formalism. For comparison, we also depict the results provided by the SRIM code [32], which are based on an interpolation, using Bragg's additivity rule, of the experimental stopping powers of Hf and O. As it can be observed, its predictions overestimate the experimental data.

The results for alpha particle beams are depicted in Fig. 5. Experimental data cover an energy range from 120 to 3000 keV that includes the maximum of the stopping power. The results obtained from the dielectric formalism with the MELF-GOS model are also represented. A quite good agreement with the experimental data is achieved in the whole energy range, in particular for the maximum stopping power. In this case, the SRIM results [32] are in reasonable agreement in the low-energy region (up to 400 keV), but for larger energies, this code slightly overestimates the experimental data. In the inset of Fig. 5, we show nonlinear calculations performed using the extended Friedel sum rule method [11]. As the ELF of the $HfO_2$ is very extended (see Fig. 2), it is not clear which value of the one-electron radius $r_s$ is more appropriate, so we model the $HfO_2$ target by $r_s$=1.35 and 1.5 a.u., which correspond to plasma frequencies of 25.6 and 30 eV, respectively (a.u. means atomic units). This nonlinear model provides a good description of the experimental data at the lower energies, underestimating the experimental results at larger energies. It is worth noting that the outer electrons described by Mermin-type ELF are 56 electrons per molecule and hence considering only valence electrons can only account for the lower incident-energy range, where less target electrons become excited. The nonlinear stopping predicts values larger than the MELF-GOS model or the SRIM code. After comparing in Figs. 4 and 5 the stopping power of proton and alpha particle beams in $HfO_2$ films provided by several theoretical models with the corresponding experimental data, it is evident that a good description of the target response spectrum (as provided by the MELF-GOS model) is necessary to correctly describe the stopping power of $HfO_2$ in a wide range of projectile energies.

## V. ENERGY LOSS CALCULATIONS FOR ELECTRON BEAMS

Due to the technological interest of $HfO_2$ for integrated devices, the transport of electrons through such a material must be well characterized, so theoretical estimations to know quantitatively how charged particles behave when moving through this material are required. In particular, the inelastic energy loss of electron beams is relevant since electrons are the projectiles used in several surface spectroscopy techniques, such as Auger electron spectroscopy (AES), reflection electron energy-loss spectroscopy (REELS), low-energy electron diffraction (LEED), x-ray photoelectron spectroscopy (XPS) [33], and electron Rutherford backscattering [34].

Taking into consideration that the stopping power (this work) and the energy-loss straggling [8] of $HfO_2$ for H and He beams present a good agreement between the experimental data and the theoretical calculations based on the dielectric formalism together with the MELF-GOS model, we applied the same formalism to evaluate the energy loss of an electron beam in $HfO_2$ films. For electron projectiles, a basic parameter is the IMFP, since it is required to interpret quantitatively surface spectroscopy techniques such as AES or XPS [35]. In the dielectric formalism, the IMFP, λ, and the stopping power, $S$, of electrons moving with velocity $v$ through a target are given by [36]

$$\lambda^{-1} = \frac{2e^2}{\hbar \pi v^2}\int_0^{\omega_{\max}} d\omega \int_{k_1}^{k_2} \frac{dk}{k}\mathrm{Im}\left[\frac{-1}{\varepsilon(k,\omega)}\right] \quad (6)$$

and

$$S = \frac{2e^2}{\pi v^2}\int_0^{\omega_{\max}} d\omega\omega \int_{k_1}^{k_2} \frac{dk}{k}\mathrm{Im}\left[\frac{-1}{\varepsilon(k,\omega)}\right], \quad (7)$$

where $k_{1,2}=mv/\hbar \mp \sqrt{(mv/\hbar)^2-2m\omega/\hbar}$, since the recoil correction is taken into account. Using the indistinguishability

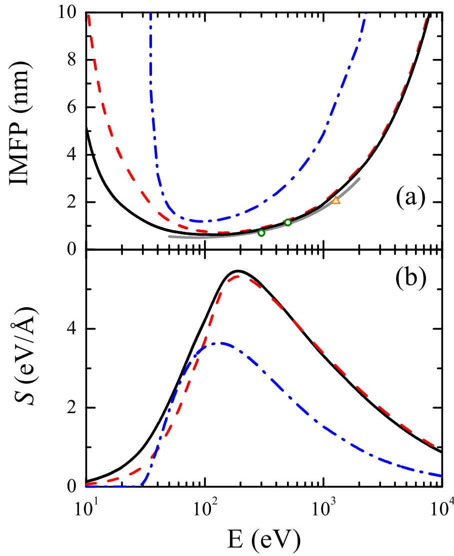


FIG. 6. (Color online) (a) Inelastic mean-free path (IMFP) and (b) stopping power of electrons in $HfO_2$ as a function of the projectile energy. The calculations have been done using the dielectric formalism and the MELF-GOS model (black solid line), the extended Drude model (dashed line), and the MELF-GOS model with a single Mermin ELF (dash-dotted line). Panel (a) also shows the results for the IMFP obtained from the TPP2 parameterization [12] (gray solid line) and the calculations from Refs. [44,45] (empty triangle) and [46] (empty circles).

criterion, i.e., the *secondary* electron is the one that emerges with smaller energy after the collision, hence the maximum energy transfer will be $\hbar\omega_{\max}=mv^2/4$.

Figure 6 depicts the theoretical predictions of (a) the IMFP and (b) the stopping power for electrons in $HfO_2$ films as a function of their energy. We show by a black solid line the results obtained with the dielectric formalism and the MELF-GOS model. These calculations predict a minimum value around 6.3 Å for the IMFP and a maximum value of 5.5 eV/Å for the stopping power, which correspond to electron energies around 120 and 190 eV, respectively.

At sufficiently high electron energies, a modified Bethe equation [36] provides an adequate description of the IMFP, $\lambda(E)$ dependence on energy, given by

$$\lambda = \frac{E}{E_p^2[\beta \ln(\gamma E) - C/E + D/E^2]}, \quad (8)$$

where the IMFP is given in nm, $E$ is the electron energy (in eV), $E_p=28.8(N_v\rho/M)^{1/2}$ is the free-electron plasmon energy (in eV), $M$ is the molecular mass, $\rho$ is the mass density of the target, $N_v$ is the number of valence electrons per molecule (for $HfO_2$ $\rho=9.68$ g/cm$^3$ and $N_v=16$ [37]), and $\beta$, $\gamma$, $C$, and $D$ are fitting parameters. Note that Eq. (8) represents a modification of Bethe equation by the inclusion of exchange effects [38] and departures from the first Born approximation [39]. We have fitted the electron IMFP obtained from the MELF-GOS model with Eq. (8), obtaining the following parameters for the $HfO_2$ target: $\beta=0.22$ eV$^{-1}$ nm$^{-1}$, $\gamma=0.056$ eV$^{-1}$, $C=15$ nm$^{-1}$, and $D=428$ eV$^{-1}$ nm$^{-1}$; this parameterization is valid at electron energies larger than 40 eV.

The Tanuma-Powell-Penn formula (TPP2) [12,13] for the electron IMFP, based on an algorithm developed by Penn [40], has been applied to a $HfO_2$ target. In Fig. 6(a), we show the TPP2 results for its valid energy range (50–2000 eV). The predictions of the TPP2 formula practically coincide with the results of the MELF-GOS model in the energy range ~200–800 eV; however as the energy moves away from this region, differences in the IMFP predictions are more sizeable due to the influence of a proper description of the $HfO_2$ ELF. Note that the fitting parameters $\beta$, $\gamma$, $C$, and $D$ for $HfO_2$ obtained from the MELF-GOS model are different from the TPP2 formula and allow the calculation of the electron IMFP even for electron energies larger than the upper limit of the TPP2 formula.

We also show the electron IMFP and stopping power obtained using an extended Drude model [41] to describe the ELF of $HfO_2$ target instead of the MELF-GOS model. Results from both models agree at high electron energies but there are significant differences at energies lower than 200 eV. The extended Drude model, although equivalent to the MELF-GOS model in the optical limit, makes an extrapolation at finite transferred momentum through a dispersion scheme that does not describe correctly the individual excitations at small momentum transfer [42,43]. Besides, we evaluate the electron IMFP and $S$ from the MELF-GOS model assuming that the $HfO_2$ excitation spectrum is given by a single Mermin-ELF (with parameters $A_1=1$, $\hbar\omega_1=30$ eV, and $\hbar\gamma_1=21.8$ eV); in this case, neither the IMFP nor $S$ agree with the other theoretical results. We remind that this simple ELF considers only 19.4 outer electrons, whereas a suitable ELF based in experimental optical ELF takes into account all the 56 outer electrons of the $HfO_2$ target. A recent calculation [44,45] of the electron IMFP for 1273 eV electrons, corresponding to the Hf $4d_{5/2}$ photoelectron line from $HfO_2$ excited by an Al $K\alpha$ x-rays source, is also included in Fig. 6; this value coincides with the TPP2 formula.

We also depict estimations of the electron IMFP based in an experimental quantitative analysis of reflection electron energy-loss spectra [46]. These results are in reasonable agreement both with the MELF-GOS model and the TPP2 formula.

In summary, we have shown that an accurate description of the excitation spectrum of the $HfO_2$ target is necessary in order to evaluate correctly the electron stopping power and related magnitudes in solids. The MELF-GOS model has the advantage that it is based on experimental optical data and uses a correct description at non-null momentum transfer given by the Mermin ELF; hence the model is able to evaluate the electron IMFP and stopping power in a wide range of incident electron energies. Therefore, the MELF-GOS method is a convenient tool to analyze dielectric materials. Unfortunately, it should be mentioned there is no available experimental data of these quantities to contrast the accuracy of these calculations.

## VI. CONCLUSIONS

The stopping power of $HfO_2$ for H and He projectiles has been measured in an energy range of from 120 to 900 keV

for proton beams and 120–3000 keV for alpha particle beams by using the RBS technique. Theoretical calculations were done using the dielectric formalism and the MELF-GOS model to account for the electronic target response. Also nonlinear calculations using the extended Friedel sum rule were included for comparison, complementing the dielectric approach and providing a good description of the experimental data in the low-energy range. The theoretical-experimental agreement is good for H ions and quite good for He ones. In both cases, the theory reproduces very well the maximum of the stopping power which usually represents a real challenge for any theoretical description. The inelastic mean-free path and stopping power of $HfO_2$ for electron beams have been calculated with the dielectric formalism and the MELF-GOS model for a wide range of incident energies, predicting the minimum IMFP and the maximum $S$ at electron energies about 120 and 190 eV, respectively.

## ACKNOWLEDGMENTS

We thank to J. M. Fernández-Varea for providing us the nonhydrogenic and relativistic GOS of the inner shells of Hf. This work has been financially supported by the Spanish Ministerio de Ciencia e Innovación (Projects No. FIS2006-13309-C02-01 and No. FIS2006-13309-C02-02) and the Brazilian CNPq Agency (Contract No. 150757/2007). C.D.D. thanks the Spanish Ministerio de Educación y Ciencia and Generalitat Valenciana for support under the Ramón y Cajal Program.

[1] P. Sigmund, *Particle Penetration and Radiation Effects: General Aspects and Stopping of Swift Point Charges* (Springer, Berlin, 2006).
[2] J.-P. Locquet, C. Marchiori, M. Sousa, J. Fompeyrine, and J. W. Seo, J. Appl. Phys. **100**, 051610 (2006).
[3] R. Katamreddy, R. Inman, G. Jursich, A. Soulet, and C. Takoudis, Thin Solid Films **516**, 8498 (2008).
[4] J. Jang, T. J. Park, J.-H. Kwon, J. H. Jang, C. S. Hwang, and M. Kim, Appl. Phys. Lett. **92**, 232906 (2008).
[5] M. F. Al-Kuhaili, Opt. Mater. **27**, 383 (2004).
[6] J. M. Khoshman and M. E. Kordesch, Surf. Coat. Technol. **201**, 3530 (2006).
[7] H. Ji, M. Yu, H. Shi, X. Shi, R. Huang, X. Zhang, J. Zhang, K. Suzuki, and H. Oka, Nucl. Instrum. Methods Phys. Res. B **226**, 537 (2004).
[8] I. Abril, M. Behar, R. Garcia-Molina, R. C. Fadanelli, L. C. C. M. Nagamine, P. L. Grande, L. Schünemann, C. D. Denton, N. R. Arista, and E. B. Saitovitch, Eur. Phys. J. D **54**, 65 (2009).
[9] I. Abril, R. Garcia-Molina, C. D. Denton, F. J. Pérez-Pérez, and N. R. Arista, Phys. Rev. A **58**, 357 (1998).
[10] S. Heredia-Avalos, R. Garcia-Molina, J. M. Fernández-Varea, and I. Abril, Phys. Rev. A **72**, 052902 (2005).
[11] A. F. Lifschitz and N. R. Arista, Phys. Rev. A **57**, 200 (1998).
[12] S. Tanuma, C. J. Powell, and D. R. Penn, Surf. Interface Anal. **17**, 911 (1991).
[13] S. Tanuma, C. J. Powell, and D. R. Penn, Surf. Interface Anal. **17**, 927 (1991).
[14] N. Bohr, K. Dan. Vidensk. Selsk. Mat. Fys. Medd. **18**, No. 8 (1948).
[15] W. K. Chu, J. W. Mayer, and M. A. Nicolet, *Backscattering Spectrometry* (Academic Press, New York, 1978).
[16] G. H. Lantschner, J. C. Eckardt, A. F. Lifschitz, N. R. Arista, L. L. Araujo, P. F. Duarte, J. H. R. dos Santos, M. Behar, J. F. Dias, P. L. Grande, C. C. Montanari, and J. E. Miraglia, Phys. Rev. A **69**, 062903 (2004).
[17] J. Lindhard, K. Dan. Vidensk. Selsk. Mat. Fys. Medd. **28**, No. 8 (1954).
[18] N. R. Arista and A. F. Lifschitz, *Advances in Quantum Chemistry. Theory of the Interaction of Swift Ions with Matter, Part 1* (Elsevier, Amsterdam, 2004), Vol. 45, p. 47.
[19] W. Brandt and M. Kitagawa, Phys. Rev. B **25**, 5631 (1982).
[20] P. L. Grande and G. Schiwietz, CASP code, Convolution Approximation for Swift Particles, version 3.1, 2005. Available at http://www.hmi.de/people/schiwietz/casp.html
[21] W. H. Bragg and R. Kleeman, Philos. Mag. **10**, 318 (1905).
[22] S. Heredia-Avalos, I. Abril, C. D. Denton, J. C. Moreno-Marín, and R. Garcia-Molina, J. Phys.: Condens. Matter **19**, 466205 (2007).
[23] C. D. Denton, I. Abril, J. C. Moreno-Marín, S. Heredia-Avalos, and R. Garcia-Molina, Phys. Status Solidi B **245**, 1498 (2008).
[24] J. C. Moreno-Marín, I. Abril, S. Heredia-Avalos, and R. Garcia-Molina, Nucl. Instrum. Methods Phys. Res. B **249**, 29 (2006).
[25] N. D. Mermin, Phys. Rev. B **1**, 2362 (1970).
[26] J. M. Fernández-Varea (private communication).
[27] J. Frandon, B. Brousseau, and F. Pradal, Phys. Status Solidi B **98**, 379 (1980).
[28] J. M. Sanz, M. A. Bañon, E. Elizalde, and F. Yubero, J. Electron Spectrosc. Relat. Phenom. **48**, 143 (1989).
[29] M. P. Agustin, L. R. C. Fonseca, J. C. Hooker, and S. Stemmer, Appl. Phys. Lett. **87**, 121909 (2005).
[30] Stopping Powers and Ranges for Protons and Alpha Particles , ICRU Report No.49 (International Commission on Radiation Units and Measurements, Bethesda, Maryland, 1994).
[31] A. F. Lifschitz and N. R. Arista, Phys. Rev. A **58**, 2168 (1998).
[32] J. F. Ziegler and J. P. Biersack, SRIM-2003. The Stopping and Range of Ions in Matter, version 2008, code available from http://www.srim.org
[33] D. P. Woodruff and T. A. Delchar, *Modern Techniques of Surface Science*, Cambridge Solid State Sciences Series (Cambridge University Press, Cambridge, England, 1994).
[34] M. R. Went and M. Vos, Nucl. Instrum. Methods Phys. Res. B **266**, 998 (2008).
[35] C. J. Powell and A. Jablonski, J. Phys. Chem. Ref. Data **28**, 19 (1999).
[36] C. J. Tung, J. C. Ashley, and R. H. Ritchie, Surf. Sci. **81**, 427 (1979).
[37] S. Tanuma, C. J. Powell, and D. R. Penn, Surf. Interface Anal. **35**, 268 (2003).
[38] M. Inokuti, Rev. Mod. Phys. **43**, 297 (1971).

[39] J. C. Ashley, J. Electron Spectrosc. Relat. Phenom. **46**, 199 (1988).
[40] D. R. Penn, Phys. Rev. B **35**, 482 (1987).
[41] R. H. Ritchie and A. Howie, Philos. Mag. **36**, 463 (1977).
[42] C. D. Denton, I. Abril, R. Garcia-Molina, J. C. Moreno-Marín, and S. Heredia-Avalos, Surf. Interface Anal. **40**, 1481 (2008).
[43] R. Garcia-Molina, I. Abril, C. D. Denton, S. Heredia-Avalos, I. Kyriakou, and D. Emfietzoglou, Nucl. Instrum. Methods Phys. Res. B **267**, 2647 (2009).
[44] C. J. Powell and A. Jablonski, Surf. Interface Anal. **38**, 1348 (2006).
[45] A. Jablonski and C. J. Powell, J. Vac. Sci. Technol. A **27**, 253 (2009).
[46] H. Jin, S. K. Oh, H. J. Kanga, and S. Tougaard, J. Appl. Phys. **100**, 083713 (2006).